On the high strain rate behavior of 63-37 Sn-Pb eutectic solders with temperature effects

Naveed Iqbal[a], Pu Xue[a], Bin Wang[b], Yulong Li[a, *]

[a]School of Aeronautics, Northwestern Polytechnical University, Xi'an, P.R China 710072

[b]School of Engineering and Design, Brunel University, Uxbridge, UB8 3PH , UK

Abstract:

This study presents experimental results performed on samples of Eutectic solder material (63 wt. % Sn 37 wt. % Pb). The tests were performed at high strain rates using Split Hopkinson's Pressure Bar (SHPB). The strain rates were in the range of $400s^{-1}$ to $1300s^{-1}$. Heating unit was added to conventional SHPB to vary initial sample temperature conditions. Tests were conducted at room temperature, 60°C and 120°C for the compressive mode, and at room temperature only for the tensile mode. The effects of temperature on the behavior of material were compared. Transient temperature changes during the dynamic loading conditions were calculated by an analytical approach using measured stress-strain data for plastic work. In addition, tests were performed in tension using Tensile Hopkinson's bar (SHTB) under the same initial temperature condition as for the compression tests. Finally, the constitutive relationship based on the Johnson Cook model was developed.

Key Words: Eutectic Solders, SHPB, SHTB, Transient Temperature, Strain rate, JC Model

Introduction

Solder joints are used extensively in integrated circuits (IC) packages, performing functions as not only electric signal channels but also structural interconnections in electronic packaging. The mechanical problems of solder joints are of pivotal significance to the reliability of packaging structures at the solder-chip and package-to-board interfaces during fabrication, shipment and operation of electrical devices. With the integration and miniaturization of portable electronic devices, interfaces are increasingly loaded at strain rates higher than those previously considered, for example, mobile phones and computers in drop impacts [1-2]. The reliability of solder joints under shock loading has become a crucial problem in electronic appliances [3-4]. Studies have been carried out to understand the processes which take place during these events, e.g. Wang et al. [5]. Measurements of the strength under strain rate loading up to $10^2 s^{-1}$ or even $10^3 s^{-1}$ were reported using split Hopkinson's pressure bar both in tension and compression modes. Constitutive relationships based on Cowper-Symonds model were obtained. However, combined influence of temperature and strain rate on the behavior of material has not been fully understood.

During impact loading, plastic deformation in the material is rapidly developed and heat is generated during the process. The heat causes the raise of temperature in the material and is dissipated to surroundings through convection, conduction and emission. When the temperature of the material is raised, temperature-dependent properties will be directly affected. Here we are concerned with the flow stress which will be of lower values at

elevated temperatures, resulting in reduced strengths. Hence, the determination of the transient temperature rise is important for system reliability and safety.

Various techniques have been applied to measure temperatures during plastic deformation. One of the methods is the embedded thermocouples (TCs) which can be used to obtain information during fast compression tests [6-8]. However, this technique has shortcomings for dynamic loading as the responding time of TCs is difficult to calibrate, and might be too slow to show real-time transient temperature increases. The second important technique often applied is the infrared thermography, which is based on the measurement of thermal radiation emitted from the surface of the specimen during the deformation [9-13]. The difficulty of this application lies in the emissivity of the material - the relative ability of its surface to emit energy by radiation, which is often an unknown *priori*, and could be changing during the deformation. In addition, the infrared technique measures the surface temperature which may not be the same inside the material.

While the technical difficulties in measurement remain to be overcome, we adopted an analytical approach to estimate the temperature increment by assuming an adiabatic process for the dynamic event where all plastic work is assumed to be converted to heat for a uniform temperature rise in the tested sample material.

In coupled thermo-mechanical problems, a relationship between strain and temperature is provided in the heat conduction equation [14]. For a given material under a uni-axial stress condition, the temperature balance can be expressed as

$$KV^2T - dT = -\frac{\beta\sigma_{ij}d\varepsilon_{ij}^{p}}{\rho C_p} + \frac{\alpha}{\rho C_p}\frac{E}{(1-2\upsilon)}T_0 d\varepsilon_{kk}^{e} \qquad (1)$$

where ρ is the material density, C_p the specific heat capacity at constant pressure, T the temperature and T_0 the initial sample temperature. α is the thermal expansion coefficient of the sample material and K the thermal diffusivity, σ_{ij} the stress components, ε_{kk}^{e} and ε_{ij}^{p} the elastic and plastic strain components, respectively, and β is the Taylor–Quinney coefficient [14] that represents the plastic work fraction converted to heat. In Hopkinson bar tests, the thermoelastic effect, $\frac{\alpha}{\rho C_p}\frac{E}{(1-2\upsilon)}T_0 d\varepsilon_{kk}^{e}$ is considered negligible, and an adiabatic condition, i.e. $KV^2T=0$, is assumed. Thus Eq. (1) becomes,

$$dT = \frac{\beta\sigma_{ij}d\varepsilon_{ij}^{p}}{\rho C_p} \qquad (2)$$

The specific heat capacity, C_p, and the density, ρ, are considered as constants during the test. For simple calculation, the factor β is treated as a constant. From the true stress-strain relationship obtained from the dynamic tests, Eq. (2) can be integrated for thermal increment as a function of the plastic strain. It has been proved experimentally [11] that the whole work done can be assumed to convert to heat, i.e. β can be taken as 1.

Experiments

To analyze the material behavior under different environmental temperatures, strain rate tests were performed in the compressive mode at ambient temperature (25°C), 60°C and 120° C which is approximately two-third of the melting temperature of the sample

material, and in the tensile mode at ambient temperature. The values of the strain rate achieved were 400, 800 and 1300 s^{-1}. Tests under each temperature were repeated five times for each strain rate and the average values were used for analysis.

Compression SHPB:

The conventional Split Hopkinson pressure bar system introduced by Kolsky [16] is consisted of an incident bar, a transmitted bar and a striker. The specimen is placed between the incident and transmission bars. When the striker hits the free end of the incident bar, a compressive stress wave is generated and propagates along the incident bar. When this wave reaches the interface of the incident bar and the specimen, part of the wave reflects back due to the impedance mismatch between the bar and the specimen, and the remaining part of the wave passes through the specimen and deforms it, then into the transmission bar. Strain gauges are used to measure the incident strain ε_i, the reflected strain ε_r, and the transmitted strain ε_t. The strain rate, strain and stress in the specimen can then be calculated from the measured strains, often by using the one dimensional stress wave theory as given in Eqs. (3) to (5).

$$\varepsilon' = -\frac{2C\varepsilon_r(t)}{L_s} \tag{3}$$

$$\varepsilon(t) = \int_0^t \varepsilon'(\tau)d\tau \tag{4}$$

$$\sigma(t) = \frac{AE\varepsilon_t(t)}{A_s} \tag{5}$$

where $C = \sqrt{\dfrac{E}{\rho}}$ is the longitudinal wave speed of the bar, in which ρ is the mass density of the bar. A and E are the cross-sectional area and Young's modulus of the bars, respectively. L_s and A_s are the length and cross-sectional area of specimen.

The SHPB used in this study consists of Maraging steel bars of diameter 12.7mm, and length 1220mm for the incident and transmission bars, and length 400mm for the striker. Copper made pulse shapers were used to ensure stress equilibrium in the specimen during loading. A schematic diagram of the setup is shown in Fig. 1. Tested samples were of diameter 5mm and length 5mm.

Temperatures of the tests were controlled by a heating unit which is consisted of a heating furnace and a thermocouple attached to the surface of the specimen to measure the temperature. When the desired temperature is achieved as indicated by the thermocouple, it was kept for 5 minutes to ensure uniformity in the sample. An illustration of heating unit attachment is shown in Fig. 2.
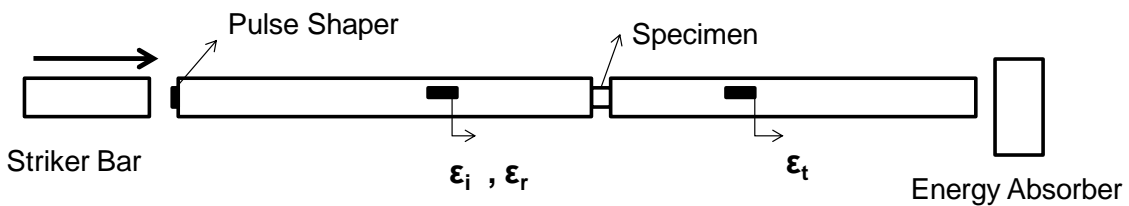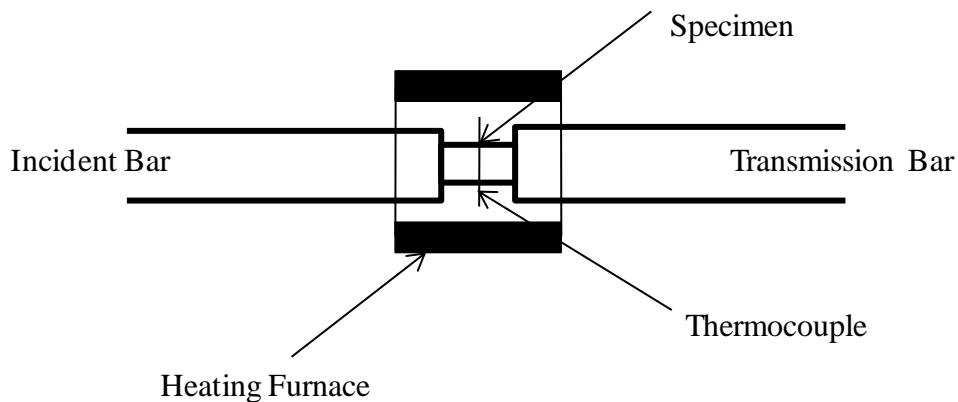

Fig.1 Schematic illustration of SHPB

Fig.2 Schematic illustration of heating unit attached with SHPB

Tensile SHB

Dynamic testing in the tension mode using a tensile SHB was developed by Harding J. et. al. [17]. A schematic illustration of the tensile bar system used in this study is shown in Fig.3. A tubular projectile is driven to strike the anvil bar which is an integral part of the incident bar at its free end. A tensile stress wave is generated and propagates along the incident bar. The rest of the process is the same as that of a compression Split Hopkinson bar. The traces of three signals are recorded as the incident, reflected and transmitted strains. Specimens used in tensile tests are of a cylindrical dog bone shape with a gauge length of 12 mm and diameter of 5mm.
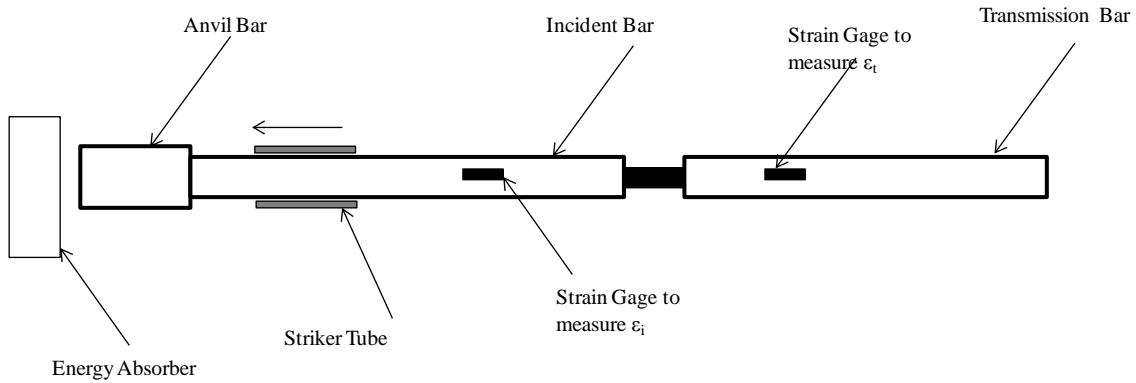
Fig.3 Schematic illustration of tensile SHB

Results

Compression tests:

The results of compression tests performed at various strain rates are shown in Figs. 4 to 6, corresponding to the room temperature, 60°C and 120 °C, respectively. It can be observed that the overall material response is approximately bilinear, with clear signs of the strain rate hardening, and thermal softening by increased test temperature.
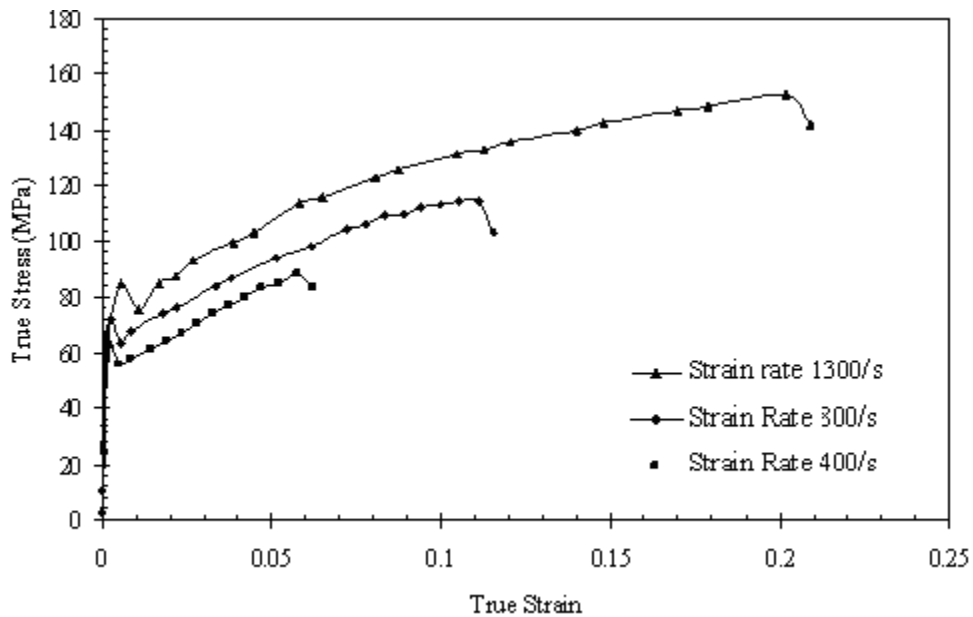
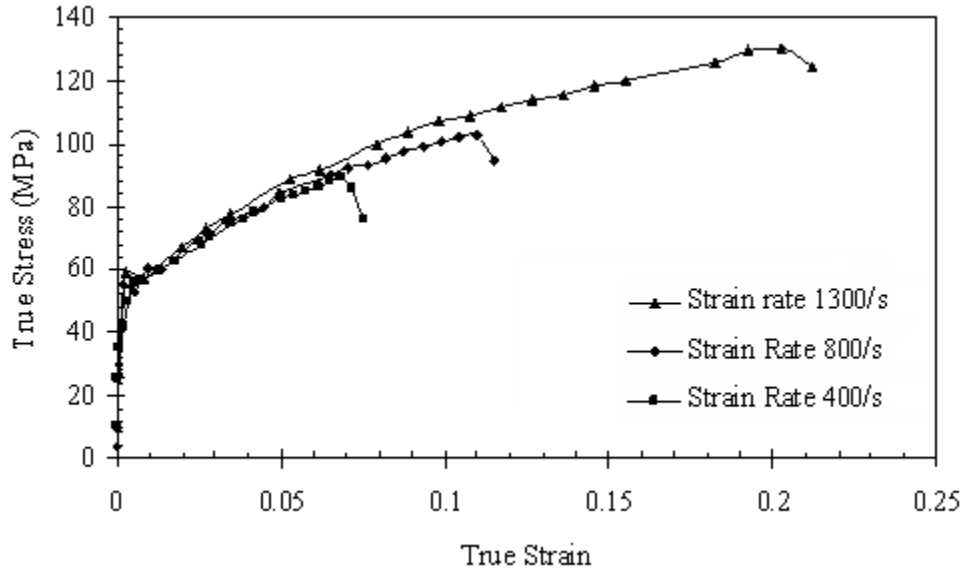Fig.4 Behavior of Sn/Pb 63/37 at room temperature
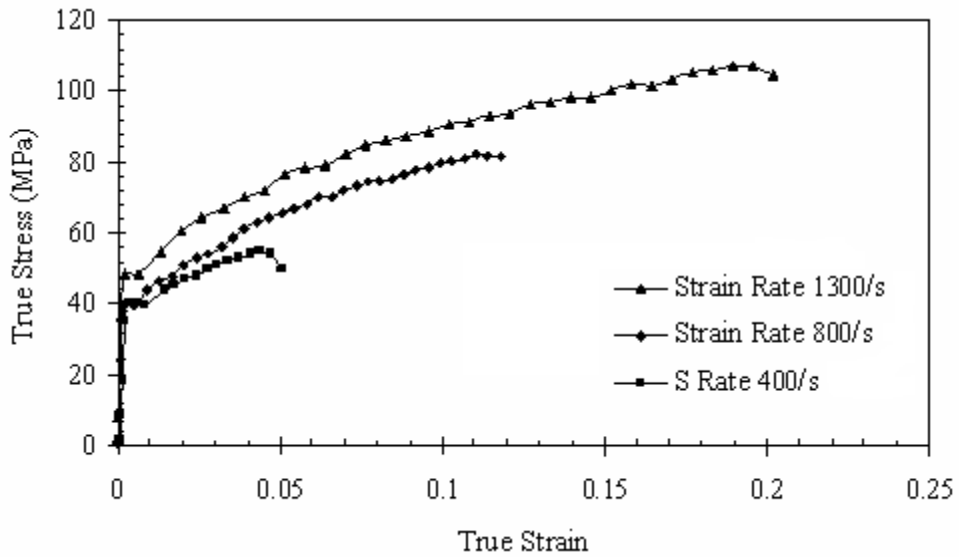

Fig.5 Behavior of Sn/Pb 63/37 at 60°C

Fig.6 Behavior of Sn/Pb 63/37 at 120°C

Tensile test results:

Figure 7 show the results of tensile SHB. Eight specimens were tested for each given strain rate. Tensile tests were performed only at the room temperature. The material shows a softening behavior after the yield point, and necking in later stages as seen in recovered samples. The starting point of necking needs to be identified as corrections for the value of the stress should be taken for the reduced cross-section area. However, the main interest of this work was on the dynamic yield stress which is not affected by necking, thus no effort was taken to trace the occurrence of necking. Curves in Fig. 7 were calculated based on an assumption of a constant cross-sectional area for the value of the dynamic yield stress. Care needs to be taken to interpret the later part with increased strains.
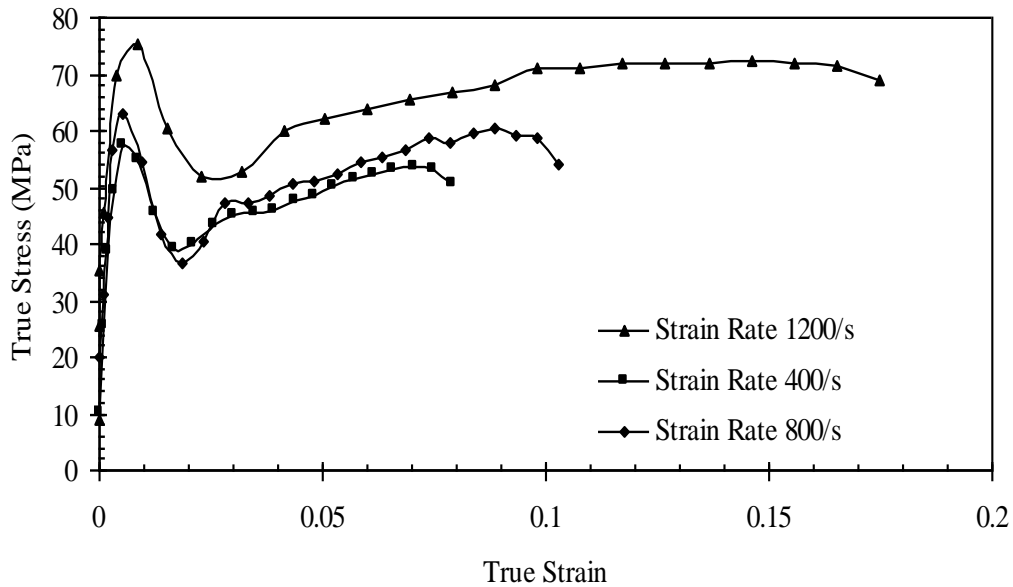

Fig.7 Behavior of Sn/Pb 63/37 using tensile SHB

Discussions

Strain rate sensitivity:

The solder material shows a clear yield point under strain rate loading, and its overall behavior is bilinear for compressive tests. The material's yield strength shows sensitivity in both the strain rate and the initial temperature. In Fig. 8, the trend of the compressive yield strength is plotted against strain rates at various initial temperatures. The behavior can be expressed approximately by a linear relationship shown in Eq. (6).

$$\sigma_Y = a_0 \dot{\varepsilon} + b_0 \qquad\qquad (6)$$

where σ_Y is the yield stress, a_0 and b_0 are constants and their values can be found by curve fitting, for instance, of 0.0167 and 60.03 at the room temperature.

Fig. 8 also shows clearly that the initial temperature affects the yield behavior of the material. The strength of the material at a low temperature is higher for both the yielding and post-yielding behaviour.

The strain rate affect can also be observed in the tensile test results, where the yield strength of the material is 58, 64 and 78MPa, respectively, at the three strain rates. Following Eq. (6), we can obtain a_0 and b_0 as 0.025 and 47.25 for an approximate linear model for the tensile yield stress.
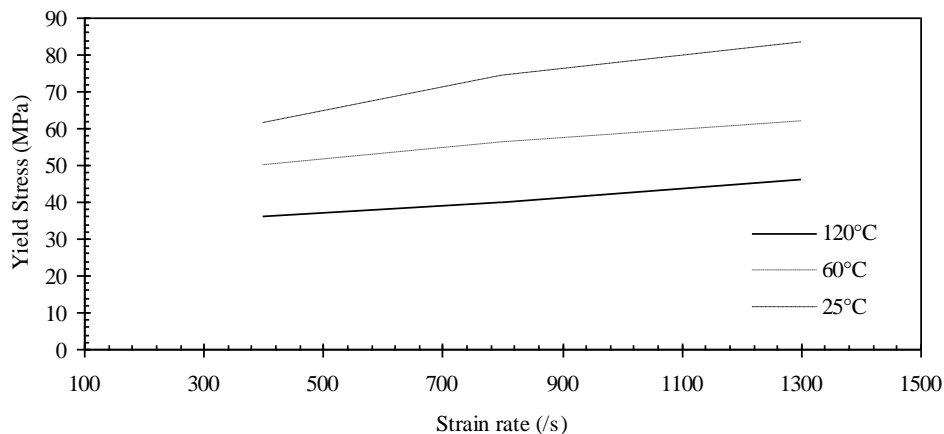
Fig.8 Yield strength of material plotted against strain rate under various
temperature conditions for compression tests

Transient temperature measurements:

Integrating Eq. (2) leads to:

$$\Delta T = \frac{\beta}{\rho C_p} \int_0^\varepsilon \sigma_{ij} d\varepsilon_{ij}^p \tag{8}$$

$\int_0^\varepsilon \sigma_{ij}\varepsilon_{ij}^p$ is the work done during the plastic deformation and can be calculated by the area

under the stress strain curves obtained from the tests.

The calculated values of the final overall temperature increase ΔT_f are given in Fig. 9.

The overall behavior can be approximated as linear over the temperature range tested. It

can be observed that ΔT_f is larger at a higher strain rate under the same temperature

condition. For instance, under the room temperature, the strain rate loading at $1300s^{-1}$

leads to an overall temperature increase of almost $17^{o}C$. The loading at $400s^{-1}$ however

yields in an increase of less than $4^{o}C$. There is also a clear trend of decrease in ΔT_f in tests

performed at a higher initial temperature condition. For the strain rate value at $1300s^{-1}$

compared with a nearly 70% temperature rise at the room temperature, tests under $120^{o}C$

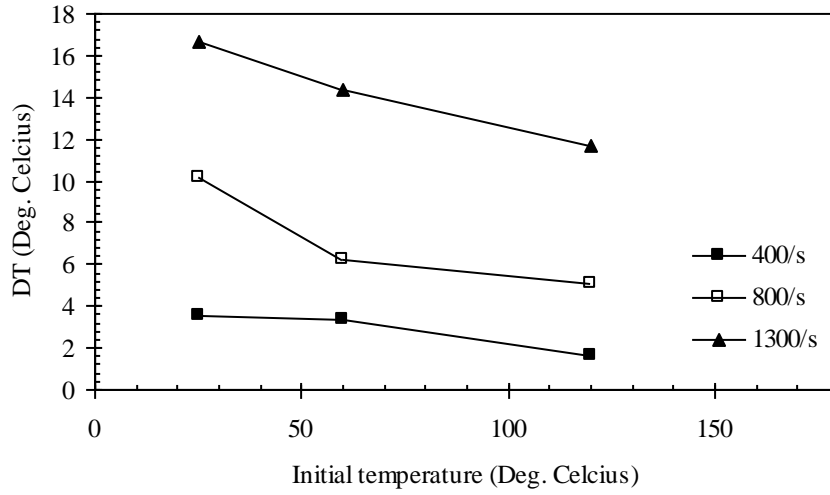yield in an overall rise of $12^{o}C$, about 10% increase only.

Fig. 9 Increase in sample temperature versus initial temperature for tests performed at various strain rates.

Johnson-Cook Model [15]

To consider the effect of both the strain rate and temperature, the semi-empirical Johnson-cook model (JC Model) is adopted, in which the flow stress is expressed as:

$$\sigma = [A + B\varepsilon^n][1 + C\ln\dot{\varepsilon}^*][1 - T^{*m}] \tag{9}$$

where σ is the flow stress, A is the yield stress at the reference strain rate, B is the coefficient of strain hardening, n the strain hardening exponent and ε the plastic strain. C is the strain rate hardening coefficient, and $\dot{\varepsilon}^* = \dot{\varepsilon}/\dot{\varepsilon}_0$, a dimensionless strain rate, defined by the ratio of $\dot{\varepsilon}$, the strain rate at T, and $\dot{\varepsilon}_0$, the reference strain rate at T_{ref}, the reference temperature. T^{*m} is the homologous temperature and is expressed as:

$$T^{*m} = \frac{T - T_{ref}}{T_m - T_{ref}}$$

with T_m being the melting temperature of the material, m the coefficient of the thermal softening exponent, respectively. The JC model considers isotropic hardening, strain rate hardening and thermal softening as three independent phenomena, where these can be isolated from each other. The total effect of strain hardening, strain rate hardening and thermal softening on the flow stress can be calculated by multiplying these three terms together, as in Eq. (9).

In the present study, the strain rate of $400s^{-1}$ at room temperature was taken as the reference strain rate. By comparing all data curves, the five parameters of JC model were identified by curve fitting and their values are shown in Table 1. The comparisons of the experimental stress-strain curves with those predicted by JC model are shown in Figs. 10 to 12.

Table 1: JC-Model parameters based on the experimental results

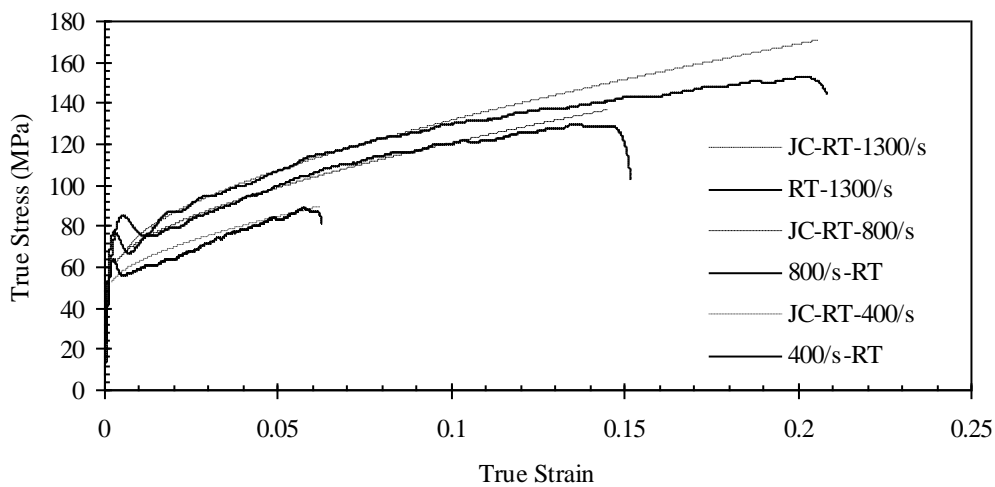| A (MPa)	B(MPa)`	n	C	m
52	220	0.65	0.29	1.95

Fig.10 Experimental and predicted stress-strain curves under room temperature conditions
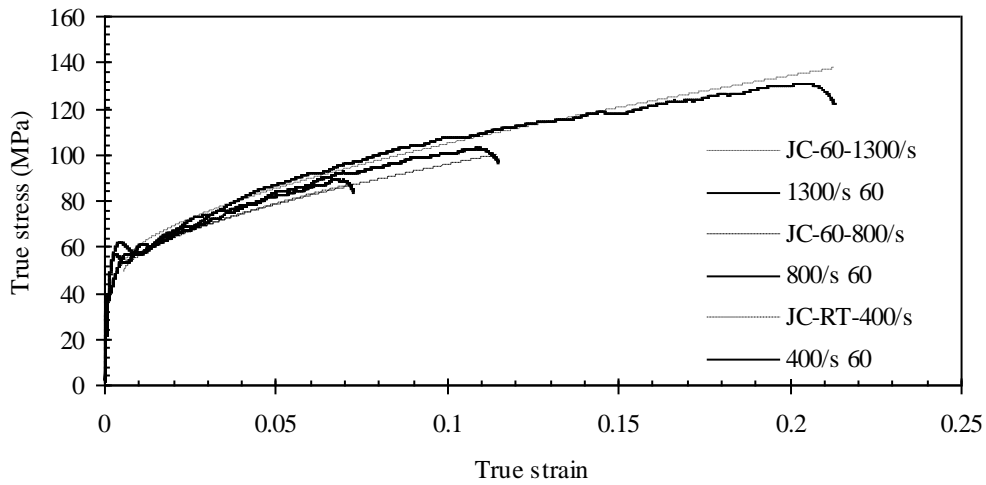
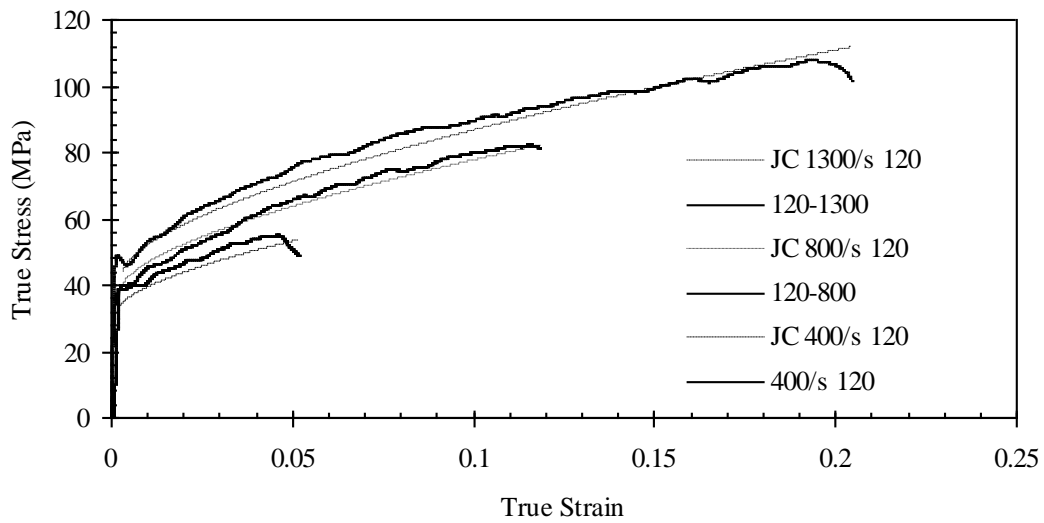Fig.11 Experimental and predicted stress-strain curves at 60°C

Fig.12 Experimental and predicted stress-strain curves at 120°C

Conclusions

The present study obtained experimental results on eutectic solder samples of 63 wt.% Sn, 37 wt.% Pb under various initial sample temperature conditions. Dynamic tests were carried out at various strain rates. The following conclusions can be drawn from the study.

1. The solder material shows sensitivity in strain rate at all temperatures tested. The initial temperature is found to have direct influence on the material's yield behavior. At a higher initial temperature, the yield strength is of a lower value under the same strain rate. The sensitivity of yield strength to the temperature can be approximated as linear.

2. Plastic deformation under the strain rate loading leads to an overall temperature increase, for which the magnitude of the increase shows a decreasing trend in terms of the initial sample temperature. The higher the initial temperature, the less the overall temperature rise (Fig. 9).

3. Dynamic loading at a higher strain rate leads to a larger temperature rise under the same initial temperature condition (Fig. 8).

4. A constitutive model based on the Johnson-Cook model has been developed, for potential use for design and analysis.

5. In general, the transient temperature rise caused by the dynamic loading is moderate at the higher temperature range (relative to the melting temperature of the material) where a 10% temperature rise may be expected. It would be interesting to look at the initial condition just below half of the material's melt temperature. Any temperature increase due to the dynamic loading may leads to glassification of the material, which may yield in changes in the mechanical properties. This remains for further study.

References:

1. Tummala, R. R., Rymaszewski, E. J., and Klopfenstein, A. G., 1997, Microelectronics Packaging Handbook, 2nd ed., Chapman and Hall, New York.

2. Tummala, R. R., 2001, "Fundamentals of Microsystems Packaging," Advances in Electronic Packaging, ASME, New York, Vol. 3, pp. 1795−1797.

3. Lim C T and Low Y J 2002 Proc. 52nd Electronics Components and Technology Conf. (San Diego, CA) (New York: IEEE) p 1270

4. Seah S K W, Lim C T, Wong E H, Tan V B C, and Shim VPW 2002 Proc. 4th Electronics Packaging Technology Conf. (Singapore) (New York: IEEE) p 120.

5. Wang B and Yi S 2002 J. Mater. Sci. Lett. Vol. 21(9), 697-698,

6. Rittel, D. (1998) Transient temperature measurement using embedded thermocouples. Exp. Mech. 38, 73−79.

7. Rittel, D. (1999) On the conversion of work to heat during high strain rate deformation of glassy polymers. Mech. Mater. 31, 131−139.

8. Rittel, D. and Rabin, Y. (2000) An investigation of the heat generated during cyclic loading of two glassy polymers. Part 2. Thermal analysis. Mech. Mater. 32, 149−159.

9. Rabin, Y. and Rittel, D. (1999) A model for the time response of solid-embedded thermocouples. Exp. Mech. 39, 133−137.

10. Haward, R. N. (1994) Heating effects in the deformation of thermoplastics. Thermochim. Acta 274, 87−109.

11. Kappor, R. and Nemat-Nasser, S. (1998) Determination of temperature rise during high strain rate deformation. Mech. Mater. 27, 1–12.

12. Manson, J. J., Rosakis, A. J. and Ravichandran, G. (1994) On the strain and strain rate dependence of the fraction of plastic work converted to heat: an experimental study using high speed infrared detectors and the Kolsky bar. Mech. Mater. 17, 135–145.

13. Rabin, Y. and Rittel, D. (2000) Infrared temperature sensing of mechanically loaded specimens: thermal analysis. Exp. Mech. 40, 197–202.

14. Taylor, G. I. and Quinney, M. A. (1934) The latent energy remaining in a metal after cold working. Proc. R. Soc. London A143, 307.

15. Gordan R. Johnson, William H. Cook, A constitutive model and data for metals subjected to large strains, high strain rates and high temperatures; Proceedings of Seventh International Symposium on Ballistics, The Hague, The Netherlands, 1983, pp. 541–547.

16. H. Kolsky, An Investigation of the Mechanical Properties of Materials at very high rates of loading, Proc. R. Soc. B62 (1949), 676-700.

17. Harding J, Wood EO, Campbell JD. Tensile testing of materials at impact rates of strain. J Mech Eng Sci 1960; 2:88–96.